Friction **11**(6): 966–976 (2023)
https://doi.org/10.1007/s40544-022-0636-3
ISSN 2223-7690
CN 10-1237/TH
RESEARCH ARTICLE

Phononic origin of structural lubrication

Yun DONG[1,†], Yongkang WANG[1,†], Zaoqi DUAN[1,†], Shuyu HUANG[1], Yi TAO[1], Xi LU[1], Yan ZHANG[1], Yajing KAN[1], Zhiyong WEI[1,*], Deyu LI[2,*], Yunfei CHEN[1,*]

[1] *Jiangsu Key Laboratory for Design and Manufacture of Micro-Nano Biomedical Instruments, School of Mechanical Engineering, Southeast University, Nanjing 211189, China*

[2] *Department of Mechanical Engineering, Vanderbilt University, Nashville 37235-1592, USA*

Received: 08 January2022 / Revised: 24 February 2022 / Accepted: 15 April 2022

Abstract: Atomistic mechanisms of frictional energy dissipation have attracted significant attention. However, the dynamics of phonon excitation and dissipation remain elusive for many friction processes. Through systematic fast Fourier transform (FFT) analyses of the frictional signals as a silicon tip sliding over a graphite surface at different angles and velocities, we experimentally demonstrate that friction mainly excites non-equilibrium phonons at the washboard frequency and its harmonics. Using molecular dynamics (MD) simulations, we further disclose the phononic origin of structural lubrication, i.e., the drastic reduction of friction force as the contact angle between two commensurate surfaces changes. In commensurate contacting states, friction excites a large amount of phonons at the washboard frequency and many orders of its harmonics that perfectly match each other in the sliding tip and substrate, while for incommensurate cases, only limited phonons are generated at mismatched washboard frequencies and few low order harmonics in the tip and substrate.

Keywords: phononic friction; washboard frequency; structural lubrication; commensurate and incommensurate interfaces

1 Introduction

Friction is ubiquitous in our world. It is not only responsible for about one-fifth of the world's total energy consumption but also the reason for the failure of most mechanical equipment with moving parts [1, 2]. Not surprisingly, tremendous efforts have been made to understand friction; and in recent decades, advanced instruments, such as atomic force microscopy (AFM), have allowed for probing friction at an atomic level that reveals intriguing phenomena [3–7]. An interesting finding is structural lubrication, which provides a convenient route to tune friction force. In 1990, based on the Frenkel–Kontorova (FK) model, Hirano and Shinjo [8, 9] predicted a fascinating friction regime in which structural incommensurability between two contacting crystalline surfaces leads to ultra-low dry friction. The finding inspired experimental endeavors to validate the proposed ultra-low friction force [10–13]. In particular, through measuring the friction between a tungsten tip with an attached graphite flake and a graphite substrate, Dienwiebel et al. [14, 15] demonstrated a sliding angle-dependent friction force, indicating superlubricity for incommensurate contacts. More recently, superlubricity between different two-dimensional (2D) materials has been observed [14–25], and it is shown that the formation of Moiré patterns [26–30] in the heterostructures is essential for superlubricity. So far, the understanding of superlubricity is from the view of mechanical interactions between incommensurate surfaces, while how structural matching affects the

† Yun DONG and Yongkang WANG contributed equally to this work.

* Corresponding authors: Zhiyong WEI, E-mail: zywei@seu.edu.cn; Deyu LI, E-mail: deyu.li@vanderbilt.edu; Yunfei CHEN, E-mail: yunfeichen@seu.edu.cn

generation of phonons, the ultimate energy carriers in friction, is still largely unknown.

Friction is essentially a process in which mechanical energy associated with the relative motion at an interface dissipates into thermal energy carried by phonons. Experimental observation of the relation between friction force and phonon generation was first reported in 1991 through a quartz crystal microbalance (QCM) measurement with sliding over adsorbed Kr monolayers [31]. More recent studies through both experimental measurements and molecular dynamics (MD) simulations disclosed the dynamics of energy dissipation during several friction processes. For example, through phonon wavepacket MD modeling, Prasad and Bhattacharya [32] found that incommensurate contacts do not necessarily result in superlubricity, but the outcome relies on the complex interactions involving longitudinal and transverse phonons. Through analyzing the vibrational density of states (VDOS) in MD simulations, Torres et al. [33] suggested that for commensurate contacts, phonons of certain low-frequency modes are preferentially excited, as evidenced by the VDOS increase at the corresponding frequency.

Very recently, our MD results demonstrated that phonons excited by friction are highly concentrated at the washboard frequency and its harmonics [34]. However, so far direct experimental evidence of this phonon excitation dynamics is still lacking. In this study, we analyze the instantaneous frictional signals as a silicon tip sliding over a graphite substrate along different crystallographic directions using the fast Fourier transform (FFT), which clearly shows that phonons are mainly excited at the washboard frequency and its harmonics. We further examine the phonon excitation process in structural lubrication and disclose the phononic origin of the drastically different friction force under commensurate and incommensurate conditions.

2 Experimental results and discussion

To experimentally demonstrate that phonons are mainly excited at the washboard frequency and its harmonics, we conducted the AFM measurements of the friction force using a sharp silicon tip of ~10 nm radius at the end. Highly-oriented pyrolytic graphite (HOPG) is chosen as the sample, which provides varying lattice periodicity corresponding to different washboard frequencies as the tip slides along different crystalline directions. The measurements were performed under ambient conditions with a temperature of 25 °C (298 K) and relative humidity of about 30%. In order to obtain the friction force along different crystallographic directions, the graphite sample is rotated manually with an increment angle of about 5°–20°, as shown in Fig. 1(a). At each rotation angle, a 5 μm × 5 μm area on the sample is selected and scanned with the AFM in the tapping mode to identify a terrace that is flat enough without any step

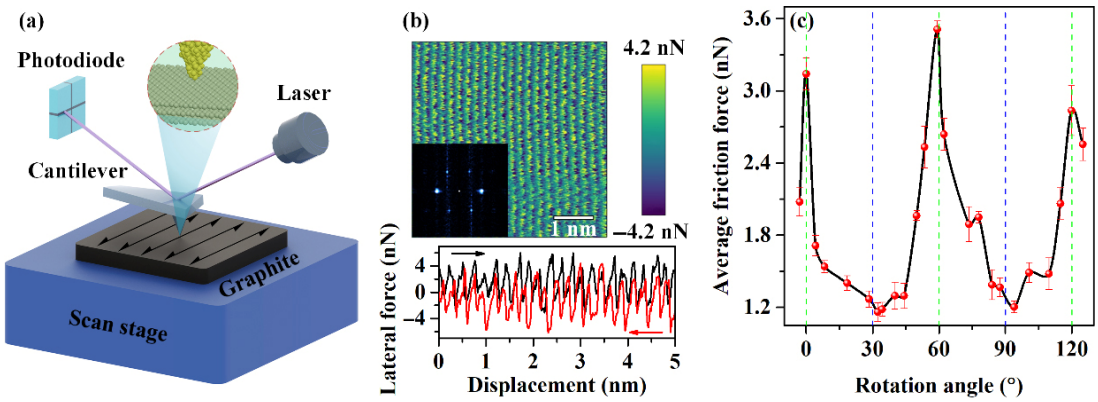

Fig. 1 (a) Schematic diagram of an AFM tip sliding over a graphite substrate. (b) 2D friction force map as the tip slides along the zigzag direction. The inset at the left bottom in (b) shows the corresponding 2D FFT of the instantaneous friction force. The bottom panel shows a typical friction loop randomly picked from the 2D friction force map in the upper panel. The forward and backward scan lines are indicated by black and red lines, respectively. (c) Average friction force vs. the sample rotation angle. Three narrow peaks of high friction forces are observed at the rotation angles of 0°, 60°, and 120°, corresponding to a sliding direction close to the armchair direction.

edges (Section S1.1 in the Electronic Supplementary Material (ESM)). Then, the AFM is switched to the contact mode with a constant normal load of 100 nN to scan a small area of 5 nm × 5 nm with the sampling points being set as 256 × 256 to observe the stick–slip pattern. Figure 1(b) shows a representative lateral force map when the sliding direction is along the zigzag direction of the graphite surface. The sliding direction can be distinguished from the 2D FFT of the instantaneous friction force as shown in the inset in Fig. 1(b). In the corresponding 2D FFT image, the position of each carbon atom in the reciprocal lattice space and the period length along the sliding direction can be directly read out [35]. The bottom panel in Fig. 1(b) presents a friction force loop that clearly reveals the resolved stick–slip motion of the tip in a forward and backward scan.

From the lateral force map, we can calculate the average friction force as the tip slides along a specific crystallographic direction. With the rotation of the sample, the resulting plot of the average friction force vs. the rotation angle is shown in Fig. 1(c), which exhibits a 60° periodicity with the maximum and minimum friction forces aligned with the scan along the direction close to the armchair and zigzag directions, respectively. In our experiment, a single-crystalline silicon probe is employed, over which a thin native oxide layer may be formed, which leads to an amorphous-crystalline tip-sample interface. As the tip slides along different crystallographic directions, the tip undergoes spatially discrete adhesion and jumps [36], i.e., it scans over different numbers of carbon atoms per unit length. The period length along different sliding directions corresponds to the period of the interaction potential between the silicon tip and the graphite substrate [37]. As shown in Fig. S2 in the ESM, the period length along different sliding directions exhibits the same 60° periodicity as that of the friction force shown in Fig. 1(c).

The FFT of the measured instantaneous friction force can disclose its spectrum distribution information. Figure 2(a) shows the FFT spectrum for the

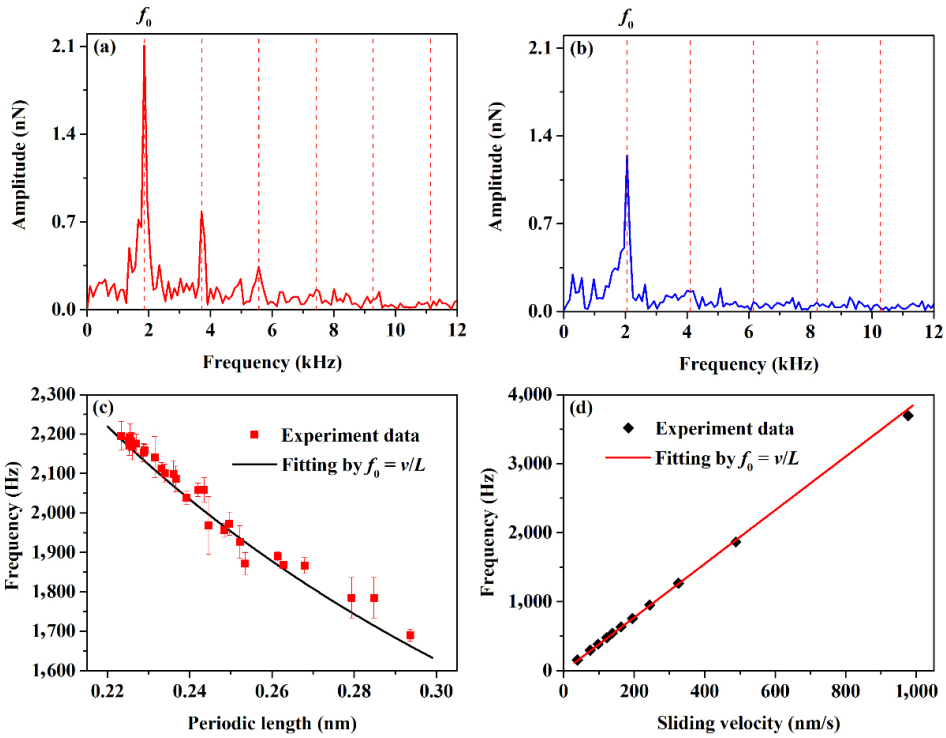

Fig. 2 FFT spectra of the instantaneous friction force at a sliding velocity of 488.25 nm/s for the sliding direction close to the (a) armchair and (b) zigzag direction. The red reference dashed lines indicate the corresponding washboard frequency and its harmonics. The period lengths along the armchair and zigzag sliding directions are determined to be L = 0.268±0.001 and 0.242±0.002 nm, respectively. (c) Variation of the first peak frequency from the FFT spectrum as a function of the periodic length along different sliding directions with a fixed sliding velocity of 488.25 nm/s. (d) Variation of the first peak frequency from the FFT spectrum as a function of the sliding velocity along a specified direction with a periodic length of 0.263±0.002 nm.

instantaneous friction force obtained at a sliding direction close to the armchair direction. Along this sliding direction, the measured period length is determined to be $L = 0.268\pm0.001$ nm, which corresponds to a washboard frequency of $f_0 = v/L = 1822.46\pm5.53$ Hz, where v is the sliding velocity. f_0 coincides almost perfectly with the first peak in the FFT spectrum, which has the largest amplitude. Besides the first peak, the second and third peaks at $2f_0$ and $3f_0$ frequencies can also be easily distinguished in the FFT spectrum. Peaks of even higher-order harmonics can be identified, but their amplitude becomes smaller with the increasing order. The distinctive peaks in the FFT spectrum indicate that the components at the washboard frequency and its harmonics make dominant contributions to the friction force. As the AFM tip slides over the graphite surface, the sliding tip interacts with the substrate carbon atoms, which induces atomic vibrations. The FFT peaks of the friction force indicate the frequencies of the excited vibrations, which are highly concentrated at the washboard frequency and its harmonics, providing experimental evidence to our prediction based on MD simulations [34]. As a comparison, when the sliding direction is close to the zigzag direction, only one peak centered at the washboard frequency with a lower amplitude can be distinguished from the FFT spectrum, as shown in Fig. 2(b). The lower FFT peak amplitude is consistent with the observed lower friction in Fig. 1(c). We also conducted the FFT analysis of the instantaneous friction force measured along other sliding directions and at different sliding velocities. Figure 2(c) depicts the variation of the first peak frequency vs. the period length along different sliding directions at a fixed sliding velocity of 488.25 nm/s, while the sliding velocity dependence of the first peak frequency is shown in Fig. 2(d). The excellent match between the first peak in the FFT spectrum and the washboard frequency for all different period lengths and the sliding velocities clearly shows that non-equilibrium phonons excited at the washboard frequency play a critical role in the friction process.

3 Simulation results and discussion

To further understand the phononic origin of the sliding-angle-dependent friction force, we performed nonequilibrium MD simulations to examine the frictional energy dissipation process under different contact scenarios. The MD model includes a piece of square graphene flake that mimics an AFM tip and a supported graphene substrate, as illustrated schematically in Figs. 3(a) and 3(b), respectively. By rotating the crystallographic angle of the graphene flake relative to the substrate, the friction interface presents different contact angles. Periodic boundary conditions are applied along the x- and y-directions, and free boundary condition along the z-direction.

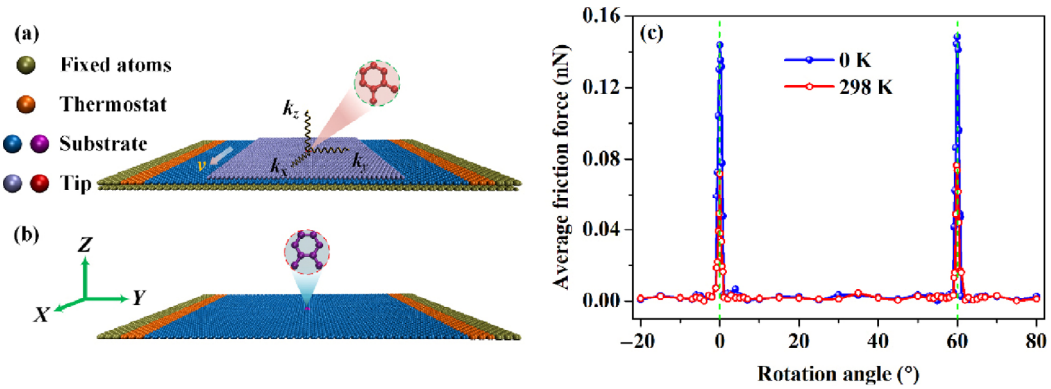

Fig. 3 (a) Friction system is composed of a piece of square graphene flake sliding along the x-axis direction over a supported graphene substrate. In the substrate, the tan atoms at the two ends of the top layer and all the bottom layer atoms are fixed without thermal vibration. In commensurate contact, both the tip and substrate are along the zigzag directions parallel with the x-axis. Three sets of springs are applied to each atom of the tip with effective spring stiffness of k_x, k_y, and k_z, which are set as 0.14, 0.08, and 0.08 N/m, respectively. (b) Only the top graphene layer of the substrate is depicted, in which the orange atoms are set as the thermostat. Eight red atoms in the tip in (a) and eight purple atoms in the substrate in (b) are selected to extract the VDOS for the tip and substrate, respectively. (c) Variation of the average friction force as a function of the tip rotation angle.

Before introducing the relative motion between the tip and substrate, the system is relaxed to thermal equilibrium with the thermostat temperature set at either 0 or 298 K. The interlayer interactions of the atoms between any two graphene layers including the tip and substrate, as well as the graphene layers in the substrate, are described by the Lennard–Jones (LJ) potential [38, 39]. The intralayer covalent bond interactions are calculated using the Tersoff potential [39, 40]. The time step used in the simulation is 0.5 fs. The properties of excited phonons are characterized by calculating the VDOS of atoms in the contacting surfaces. All MD simulations are conducted with LAMMPS software [41]. More details of the simulation model can be found in Section S1.2 in the ESM.

Figure 3(c) plots the resulting average friction force when the sliding velocity is set at 9 m/s, and the thermostat temperature at 0 and 298 K. The obtained friction force exhibits a 60° periodicity with the rotation angle, consistent with the experimentally measured trend shown in Fig. 1(c). It is worth noting that while at 298 K the peak value of the friction force is significantly lower than the corresponding value at 0 K, the sliding-angle dependence is the same for both cases.

We further calculate the average friction forces for commensurate and incommensurate contacts when the sliding velocity ramps from 5 to 55 m/s with the thermostat temperature set at 298 K, as shown in Fig. 4(a). For incommensurate contacts, the friction force is very low and hardly changes as the sliding velocity increases. However, for commensurate contacts, the average friction force increases first slowly, and then rapidly with the velocity.

Figure 4(a) also indicates that the friction force for commensurate contacts is always larger than that for incommensurate cases, which means that more mechanical energy is dissipated into heat, and one would expect a higher temperature rise of the tip and substrate under commensurate conditions. Interestingly, however, Fig. 4(b) indicates a much higher tip temperature for the incommensurate case, which is completely counter-intuitive. To further examine this unexpected result, we calculated the temperature difference between the tip and substrate, as plotted in Fig. 4(c), which also shows a larger difference for the

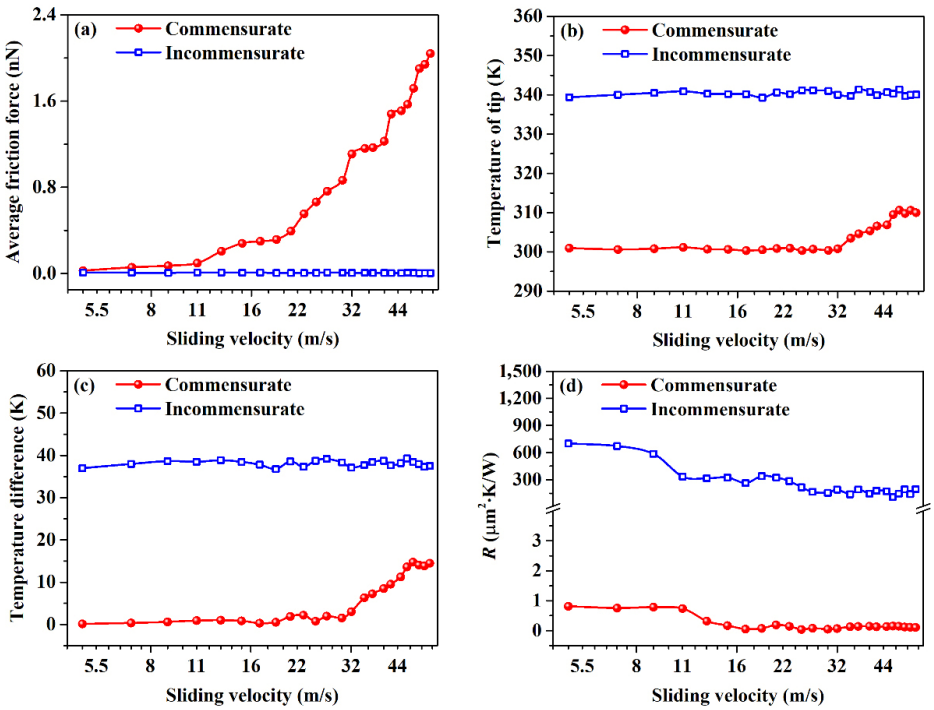

Fig. 4 (a) Average friction force as a function of the sliding velocity in commensurate and incommensurate contacts. The thermostat temperature is set at 298 K, and the specific incommensurate contact in this plot corresponds to a rotation angle of 30°. (b) Tip temperature as a function of sliding velocity. (c) Temperature difference between the tip and substrate at different sliding velocities. (d) Interfacial thermal resistance R vs. sliding velocity.

incommensurate case. Since the thermostat is placed on the substrate, a higher temperature difference between the tip and substrate suggests that it is more difficult for heat to transfer from the tip to the substrate for incommensurate contacts. The interfacial thermal resistance R can be estimated from the heat flux through the interface and the temperature difference between the tip and substrate (the detailed calculation of R in the friction process is provided in Section S1.3 in the ESM). It is found that R values at all sliding velocities for the incommensurate contact are about three orders of magnitude higher than those for the commensurate contact, as shown in Fig. 4(d). This is drastically different from the case of a static contact, for which it has been shown that while lattice mismatch caused by the relative rotation of the two contact surfaces can change R, the maximum difference of R between different rotation angles is no more than 50% [42]. We also calculate the corresponding average friction force, tip temperature, temperature difference, and R in commensurate and incommensurate contacts when the thermostat temperature is set at 0 K (Fig. S4 in the ESM). The simulation results at 0 K keep the similar trends to those at 298 K. To elucidate the underlying mechanism of the unexpected drastic difference in R corresponding to commensurate and incommensurate contacts, we extract the phonon spectra for the tip and substrate.

Figure 5 displays the VDOS of the selected atoms in the tip and substrate shown in Fig. 3(a), which reflects the populations of the vibration modes at different frequencies [43]. The discrete vibration modes as illustrated in the VDOS indicate that the phonons excited by friction are highly non-equilibrium ones concentrated at the washboard frequency and its harmonics. It should be noted that each atom on the contacting surfaces feels the potential of its opposite surface. If we calculate the washboard frequency $f_0 = v/L$ of the tip, L stands for the substrate potential period along the relative sliding direction and vice versa. For the peak friction force, the period length for the substrate potential along the sliding (zigzag) direction is $\sqrt{3}a$ (a is the C–C bond length). Once the tip is rotated 30°, the period length for the tip potential along the sliding (armchair) direction changes to $3a$ (Fig. S3 in the ESM). Note that to clearly observe the friction excited phonon modes in these calculations, the thermostat temperature is set to be 0 K to avoid complications from the background thermal phonons at elevated temperatures.

As shown in Fig. 5(a), for commensurate contacts, the frequencies of the excited phonons in the tip are the same as those in the substrate because the tip and substrate have the same lattice structure along the sliding direction. However, for incommensurate contacts, the atoms on the tip and substrate feel the potential with different period lengths due to the lattice mismatch between the tip and substrate. Consequently, the excited phonon modes in the tip and substrate have different frequencies, as illustrated

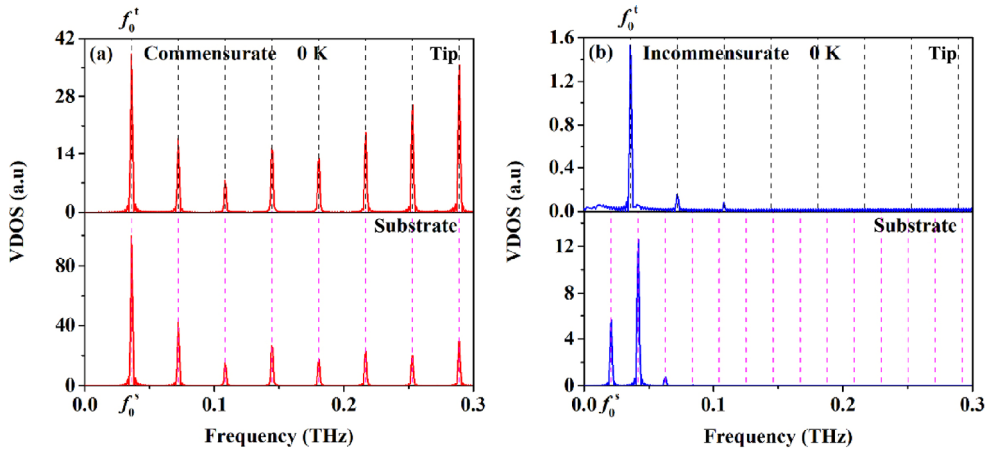

Fig. 5 Phonon spectra of the tip and substrate in the friction process with the thermostat temperature set at 0 K to clearly observe the friction excited phonon modes without the complications from the background thermal phonons, for (a) commensurate contact and (b) incommensurate contact. The dotted lines represent the washboard frequencies and their harmonics. f_0^{t} and f_0^{s} stand for the washboard frequencies for the tip and substrate, respectively.

in Fig. 5(b). These observations disclose the underlying mechanism for the large temperature difference between the tip and substrate shown in Fig. 4(c). For commensurate contacts, the excited phonon modes with overlapping frequencies in the tip and substrate offer smooth energy dissipation channels. In this case, the dissipated energy due to friction can be effectively transferred from the tip to substrate, and absorbed by thermostat. This renders both the temperature rise of the tip and the temperature difference between the tip and substrate very low. In contrast, the excited phonons in the tip have different frequencies from those on the substrate for the incommensurate contact. The mismatch of the excited phonon modes renders it difficult to transfer the atomic vibration energy from the tip to substrate, leading to the significant temperature rise of the tip.

An interesting finding is that the amplitude of the VDOS for each peak for the commensurate contact in Fig. 5(a) is about 10 to 20 times higher than that of the incommensurate case in Fig. 5(b). Importantly, besides the huge difference in the peak amplitude, the frequency range of the excited phonon modes also changes dramatically for different contact conditions. For commensurate contacts, non-equilibrium phonon modes up to the 8th harmonics of the washboard frequency can still be excited in both the tip and substrate. In contrast, it is difficult to discern the phonon modes beyond the 3rd harmonic of the washboard frequency in both the tip and substrate for the incommensurate contact. These differences suggest that for commensurate contacts, friction excites much more phonons than those in incommensurate contacts (Section S1.4 in the ESM), which provides a quantitative explanation of structure lubrication from the viewpoint of phonon excitation. With the increase of those perfectly matched phonon modes being excited, the thermal vibration energy of atoms can be effectively exchanged between the tip and substrate in commensurate contacts, resulting in a small interface temperature difference in Fig. 4(c).

4 Conclusions

In summary, the systematic study provides solid experimental evidence that friction directly excites excess non-equilibrium phonons mainly at the washboard frequency and its harmonics. Comparison of the excited phonon modes in commensurate and incommensurate contacts suggests that much more phonons are produced under commensurate condition. The results show that the overlapping frequencies of the phonons in the tip and substrate allow for smooth exchange of phonons, leading to a low interfacial thermal resistance and temperature difference between the tip and substrate. On the contrary, the mismatch of phonon spectra in incommensurate contact renders weak coupling between the excited phonons in the tip and substrate, causing three orders of magnitude high interfacial thermal resistance. The disclosed phononic origin of friction force in structural lubrication provides insights into the energy dissipation process in sliding friction.

Acknowledgements

The authors thank the National Natural Science Foundation of China (Grant Nos. 52035003, 52065037, 51575104, and 52175161), the China Postdoctoral Science Foundation (Grant No. 2021MD703810), the Postdoctoral Science Foundation of Gansu Academy of Sciences (Grant No. BSH202101), and the Southeast University "Zhongying Young Scholars" Project for financial support.

Declaration of competing interest

The authors have no competing interests to declare that are relevant to the content of this article.

Electronic Supplementary Material Supplementary material is available in the online version of this article at https://doi.org/10.1007/s40544-022-0636-3.

References

[1] Zhang S, Ma T B, Erdemir A, Li Q Y. Tribology of two-dimensional materials: From mechanisms to modulating strategies. *Mater Today* **26**: 67–86 (2019)

[2] Wang K Q, Ouyang W G, Cao W, Ma M, Zheng Q S. Robust superlubricity by strain engineering. *Nanoscale* **11**(5): 2186–2193 (2019)

[3] Gnecco E, Bennewitz R, Gyalog T, Loppacher C, Bammerlin M, Meyer E, Guntherodt H J. Velocity dependence of atomic friction. *Phys Rev Lett* **84**(6): 1172–1175 (2000)

[4] Krylov S Y, Jinesh K B, Valk H, Dienwiebel M, Frenken J W M. Thermally induced suppression of friction at the atomic scale. *Phys Rev E* **71**(6): 065101 (2005)

[5] Jansen L, Hölscher H, Fuchs H, Schirmeisen A. Temperature dependence of atomic-scale stick–slip friction. *Phys Rev Lett* **104**(25): 256101 (2010)

[6] Riedo E, Gnecco E, Bennewitz R, Meyer E, Brune H. Interaction potential and hopping dynamics governing sliding friction. *Phys Rev Lett* **91**(8): 084502 (2003)

[7] Socoliuc A, Gnecco E, Maier S, Pfeiffer O, Baratoff A, Bennewitz R, Meyer E. Atomic-scale control of friction by actuation of nanometer-sized contacts. *Science* **313**(5784): 207–210 (2006)

[8] Shinjo K, Hirano M. Dynamics of friction: Superlubric state. *Surf Sci* **283**(1–3): 473–478 (1993)

[9] Hirano M, Shinjo K. Atomistic locking and friction. *Phys Rev B* **41**(17): 11837–11851 (1990)

[10] Hirano M, Shinjo K, Kaneko R, Murata Y. Anisotropy of frictional forces in muscovite mica. *Phys Rev Lett* **67**(19): 2642–2645 (1991)

[11] Hirano M, Shinjo K. Superlubricity and frictional anisotropy. *Wear* **168**(1–2): 121–125 (1993)

[12] Martin J M, Donnet C, Le Mogne T, Epicier T. Superlubricity of molybdenum disulphide. *Phys Rev B* **48**(14): 10583–10586 (1993)

[13] Hirano M, Shinjo K, Kaneko R, Murata Y. Observation of superlubricity by scanning tunneling microscopy. *Phys Rev Lett* **78**(8): 1448–1451 (1997)

[14] Dienwiebel M, Verhoeven G S, Pradeep N, Frenken J W M, Heimberg J A, Zandbergen H W. Superlubricity of graphite. *Phys Rev Lett* **92**(12): 126101 (2004)

[15] Dienwiebel M, Pradeep N, Verhoeven G S, Zandbergen H W, Frenken J W M. Model experiments of superlubricity of graphite. *Surf Sci* **576**(1–3): 197–211 (2005)

[16] Li J F, Li J J, Jiang L, Luo J B. Fabrication of a graphene layer probe to measure force interactions in layered heterojunctions. *Nanoscale* **12**(9): 5435–5443 (2020)

[17] Liu S W, Wang H P, Xu Q, Ma T B, Yu G, Zhang C H, Geng D C, Yu Z W, Zhang S G, Wang W Z, et al. Robust microscale superlubricity under high contact pressure enabled by graphene-coated microsphere. *Nat Commun* **8**: 14029 (2017)

[18] Li J J, Gao T Y, Luo J B. Superlubricity of graphite induced by multiple transferred graphene nanoflakes. *Adv Sci* **5**(3): 1700616 (2018)

[19] Liu Y M, Wang K, Xu Q, Zhang J, Hu Y Z, Ma T B, Zheng Q S, Luo J B. Superlubricity between graphite layers in ultrahigh vacuum. *ACS Appl Mater Interfaces* **12**(38): 43167–43172 (2020)

[20] Feng X F, Kwon S, Park J Y, Salmeron M. Superlubric sliding of graphene nanoflakes on graphene. *ACS Nano* **7**(2): 1718–1724 (2013)

[21] Song Y M, Mandelli D, Hod O, Urbakh M, Ma M, Zheng Q S. Robust microscale superlubricity in graphite/hexagonal boron nitride layered heterojunctions. *Nat Mater* **17**(10): 894–899 (2018)

[22] Büch H, Rossi A, Forti S, Convertino D, Tozzini V, Coletti C. Superlubricity of epitaxial monolayer WS_2 on graphene. *Nano Res* **11**(11): 5946–5956 (2018)

[23] Liu Z, Yang J R, Grey F, Liu J Z, Liu Y L, Wang Y B, Yang Y L, Cheng Y, Zheng Q S. Observation of microscale superlubricity in graphite. *Phys Rev Lett* **108**(20): 205503 (2012)

[24] Sha T D, Pang H, Fang L, Liu H X, Chen X C, Liu D M, Luo J B. Superlubricity between a silicon tip and graphite enabled by the nanolithography-assisted nanoflakes tribo-transfer. *Nanotechnology* **31**(20): 205703 (2020)

[25] Liu Y M, Song A S, Xu Z, Zong R L, Zhang J, Yang W Y, Wang R, Hu Y Z, Luo J B, Ma T B. Interlayer friction and superlubricity in single-crystalline contact enabled by two-dimensional flake-wrapped atomic force microscope tips. *ACS Nano* **12**(8): 7638–7646 (2018)

[26] Wang K Q, Qu C Y, Wang J, Ouyang W G, Ma M, Zheng Q S. Strain engineering modulates graphene interlayer friction by Moiré pattern evolution. *ACS Appl Mater Interfaces* **11**(39): 36169–36176 (2019)

[27] Woods C R, Britnell L, Eckmann A, Ma R S, Lu J C, Guo H M, Lin X, Yu G L, Cao Y, Gorbachev R V, et al. Commensurate–incommensurate transition in graphene on hexagonal boron nitride. *Nat Phys* **10**(6): 451–456 (2014)

[28] Dong Y, Duan Z Q, Tao Y, Wei Z Y, Gueye B, Zhang Y, Chen Y F. Friction evolution with transition from commensurate to incommensurate contacts between graphene layers. *Tribol Int* **136**: 259–266 (2019)

[29] Zheng X H, Gao L, Yao Q Z, Li Q Y, Zhang M, Xie X M, Qiao S, Wang G, Ma T B, Di Z F, et al. Robust ultra-low-friction state of graphene via moiré superlattice confinement. *Nat Commun* **7**: 13204 (2016)

[30] Ouyang W G, Ma M, Zheng Q S, Urbakh M. Frictional properties of nanojunctions including atomically thin sheets. *Nano Lett* **16**(3): 1878–1883 (2016)

[31] Krim J, Solina D, Chiarello R. Nanotribology of a Kr monolayer: A quartz-crystal microbalance study of atomic-scale friction. *Phys Rev Lett* **66**(2): 181–184 (1991)

[32] Prasad M V D, Bhattacharya B. Phononic origins of friction in carbon nanotube oscillators. *Nano Lett* **17**(4): 2131–2137 (2017)

[33] Torres E S, Gonçalves S, Scherer C, Kiwi M. Nanoscale sliding friction versus commensuration ratio: Molecular dynamics simulations. *Phys Rev B* **73**(3): 035434 (2006)

[34] Duan Z Q, Wei Z Y, Huang S Y, Wang Y K, Sun C D, Tao Y, Dong Y, Yang J K, Zhang Y, Kan Y J, et al. Resonance in atomic-scale sliding friction. *Nano Lett* **21**(11): 4615–4621 (2021)

[35] Almeida C M, Prioli R, Fragneaud B, Cançado L G, Paupitz R, Galvão D S, de Cicco M, Menezes M G, Achete C A, Capaz R B. Giant and tunable anisotropy of nanoscale friction in graphene. *Sci Rep* **6**: 31569 (2016)

[36] Fujisawa S, Kishi E, Sugawara Y, Morita S. Atomic-scale friction observed with a two-dimensional frictional-force microscope. *Phys Rev B* **51**(12): 7849–7857 (1995)

[37] Morita S, Fujisawa S, Sugawara Y. Spatially quantized friction with a lattice periodicity. *Surf Sci Rep* **23**(1): 1–41 (1996)

[38] Lebedeva I V, Knizhnik A A, Popov A M, Ershova O V, Lozovik Y E, Potapkin B V. Fast diffusion of a graphene flake on a graphene layer. *Phys Rev B* **82**(15): 155460 (2010)

[39] Dong Y, Wang F Q, Zhu Z X, He T J. Influences of out-of-plane elastic energy and thermal effects on friction between graphene layers. *AIP Adv* **9**(4): 045213 (2019)

[40] Lindsay L, Broido D A. Optimized Tersoff and Brenner empirical potential parameters for lattice dynamics and phonon thermal transport in carbon nanotubes and graphene. *Phys Rev B* **81**(20): 205441 (2010)

[41] Plimpton S. Fast parallel algorithms for short-range molecular dynamics. *J Comput Phys* **117**(1): 1–19 (1995)

[42] Ren W J, Ouyang Y L, Jiang P F, Yu C Q, He J, Chen J. The impact of interlayer rotation on thermal transport across graphene/hexagonal boron nitride van der Waals heterostructure. *Nano Lett* **21**(6): 2634–2641 (2021)

[43] Dong Y, Tao Y, Feng R C, Zhang Y, Duan Z Q, Cao H. Phonon dissipation in friction with commensurate–incommensurate transition between graphene membranes. *Nanotechnology* **31**(28): 285711 (2020)

Yun DONG. He received his M.S. and Ph.D. degrees in mechanical engineering from Guangxi University and Southeast University, China, in 2010 and 2020, respectively. He has worked in Lanzhou University of Technology since 2010 as a lecture, postdoctoral fellow, and associate professor. His research areas include the structural lubrication and phononic friction.

Yongkang WANG. He received his bachelor's degree in mechanical engineering from China University of Mining and Technology, Xuzhou, China, in 2016. After then, he is a Ph.D. student in mechanical engineering at Southeast University, Nanjing, China. His research interests include solid–liquid interface and nonlinear spectroscopy.

Zaoqi DUAN. He received his Ph.D. degree in mechanical engineering of Southeast University, China, in 2021. After that, he has worked in Southeast University as a postdoctoral fellow. His research areas include nanotribology and active control friction.

Shuyu HUANG. She received her bachelor's degree in mechanical engineering from Southeast Jiaotong University, China, in 2017. After then, she is a Ph.D. student in the Jiangsu Key Laboratory for Design and Manufacture of Micro-Nano Biomedical Instruments, School of Mechanical Engineering, Southeast University, China. Her main research topic includes atomic sliding friction of two-dimensional layered materials and dynamics of frictional energy dissipation.

Yi TAO. He received his bachelor's and Ph.D. degrees in mechanical engineering from Southeast University, China, in 2014 and 2021, respectively. He has continued his work in Southeast University since 2022 as a postdoc. His research interests include phononic friction and phonon transport.

Xi LU. He received his M.S. degree in mechanical engineering from Shanghai Jiaotong University, China, in 1996, and received his Ph.D. degree in mechanical engineering from Southeast University, China, in 2006. He joined the School of Mechanical Engineering, Southeast University from 1996. His current position is an associate professor. His research areas cover computational structure dynamics and optimization design.

Yan ZHANG. She received her M.S. and Ph.D. degrees in Southeast University, China, in 2006 and 2013, respectively. She has worked in Southeast University since 1999 as a lecture and associate professor. Her research interests include the origin of friction and active control friction.

Yajing KAN. He received his B.S. and Ph.D. degrees in Southeast University, China, in 2007 and 2015, respectively. He has worked in Southeast University since 2015 as a lecture and associate professor. His research interests include the intermolecular and surface forces, interfacial structures, and bio-adhesion mechanisms.

Zhiyong WEI. He received his B.S. degree in mechanical engineering from Huazhong Agricultural University, China, in 2007, and Ph.D. degree in mechanical engineering from Southeast University, China, in 2014. He had a two-year visiting experience at the University of California, Berkeley, USA, from 2010 to 2012 supported by the China Scholarship Council (CSC) Joint Training Program. He joined the School of Mechanical Engineering, Southeast University in 2014. His current position is an associate professor. His research interests include nanotribology, phonon transport, and the areas related to friction and heat.

Deyu LI. He received his B.S., M.S., and Ph.D. degrees from University of Science and Technology of China, Tsinghua University, China, and University of California, Berkeley, USA, respectively. He is currently a professor in the Department of Mechanical Engineering at Vanderbilt University, USA. His research interests include phonon transport, microfluidics and nanofluidics, and atomic scale friction.

Yunfei CHEN. He received his M.S. and Ph.D. degrees in mechanical engineering from Hefei Polytechnic University and Southeast University, China, in 1988 and 1991, respectively. He has worked in Southeast University since 1991 as a lecture, associate professor, and full professor. His research interests include the origin of friction, active control friction, and the areas related with friction such as MEMS, superfluidics, and nanosensors.